Late Pleistocene fault slip rate, earthquake recurrence, and recency of slip along the Pyramid Lake fault zone, northern Walker Lane, United States

Richard W. Briggs and Steven G. Wesnousky
Center for Neotectonic Studies, University of Nevada, Reno, Nevada, USA

Received 31 July 2003; revised 23 March 2004; accepted 23 April 2004; published 4 August 2004.

[1] Up to 25% of Pacific-North America plate relative transform motion is accommodated east of the Sierra Nevada. Most of that 25% is taken up by deformation in the Walker Lane, a discontinuous zone of strike-slip and normal faults approximately parallel to the San Andreas. The Pyramid Lake fault zone is a northwest trending right-lateral fault in the northern Walker Lane, Nevada. Recent geodetic surveys report 6 ± 2 mm/year of right-lateral shear strain accumulation across the northern Walker Lane. Interpretation of displaced geomorphic features preserved in post-Lake Lahontan (~15,500 cal. yr B.P.) surfaces indicate the Pyramid Lake fault zone has accommodated at least 2.6 ± 0.3 mm/year of right-lateral shear during the late Pleistocene. Additionally, a minimum of two earthquakes have occurred since deposition of the Mazama tephra (~7630 cal. yr B.P.), and at least four earthquakes have occurred on the fault after desiccation of Lake Lahontan (~15.5 ka), with the most recent earthquake occurring after 1705 ± 175 cal. yr B.P. The observations indicate that the Pyramid Lake fault zone accommodates the major portion (≥25%–70%) of right-lateral slip east of the Sierra Nevada at the latitude of ~39°45′N. *INDEX TERMS:* 7221 Seismology: Paleoseismology; 8107 Tectonophysics: Continental neotectonics; 8110 Tectonophysics: Continental tectonics—general (0905); 8150 Tectonophysics: Plate boundary—general (3040); *KEYWORDS:* Walker Lane, slip rate, Pyramid Lake

Citation: Briggs, R. W., and S. G. Wesnousky (2004), Late Pleistocene fault slip rate, earthquake recurrence, and recency of slip along the Pyramid Lake fault zone, northern Walker Lane, United States, *J. Geophys. Res.*, *109*, B08402, doi:10.1029/2003JB002717.

1. Introduction

[2] Crustal deformation resulting from relative Pacific-North America plate motion is broadly distributed on faults across the western United States [*Atwater*, 1970]. Most of the transform motion is taken up on the San Andreas fault system with the remainder distributed to the east [*Minster and Jordan*, 1987]. The Walker Lane [*Stewart*, 1988] is a complex zone of discontinuous and active strike-slip and normal faults located east of the Sierra Nevada at the western margin of the Basin and Range, subparallel to the San Andreas system (Figure 1a). Geodetic observations now show that up to 25% of relative Pacific-North America transform motion is currently accommodated by faults east of the Sierra Nevada, with most of the displacement focused in the westernmost Basin and Range and Walker Lane [*Bennett et al.*, 2003; *Miller et al.*, 2001; *Gan et al.*, 2000; *Thatcher et al.*, 1999]. Neotectonic studies of fault slip rate generally account for the rates of strain accumulation documented geodetically along the San Andreas [*Ward*, 1998]. Here we attempt to determine the portion of geodetically observed strain accumulation in the northern Walker Lane that is accommodated by slip on the Pyramid Lake fault zone (Figure 1).

[3] The Pyramid Lake fault zone is a northwest trending right-lateral strike-slip fault located in the northern Walker Lane (Figure 1) [*Bonham and Slemmons*, 1968; *Bell and Slemmons*, 1979; *Bell*, 1984; *Anderson and Hawkins*, 1984]. The northern Walker Lane is a region of NW directed late Cenozoic shear located between the Basin and Range and the Sierra Nevada [*Stewart*, 1988; *Yount et al.*, 1993] and comprises a complex zone of northwest trending right-lateral strike-slip faults, northeast trending left-lateral strike-slip faults, and north trending normal faults (Figure 1). Global Positioning System (GPS) geodetic measurements indicate that the equivalent of 6 ± 2 mm/year of NW directed right-lateral shear, or 10–15% of Pacific-North America relative plate motion, is accumulating across the northern Walker Lane at ~39°–40°N. [*Thatcher*, 2003; *Thatcher et al.*, 1999; *Svarc et al.*, 2002; *Dixon et al.*, 2000]. It is only for the Honey Lake fault zone (Figure 1) that a strike-slip rate estimate based on geologic offset of Holocene deposits has been determined [*Wills and Borchardt*, 1993]. In this paper, we present Quaternary surface mapping and paleoseismic investigations along the Pyramid Lake fault zone and use our observations to place

0148-0227/04/2003JB002717$09.00

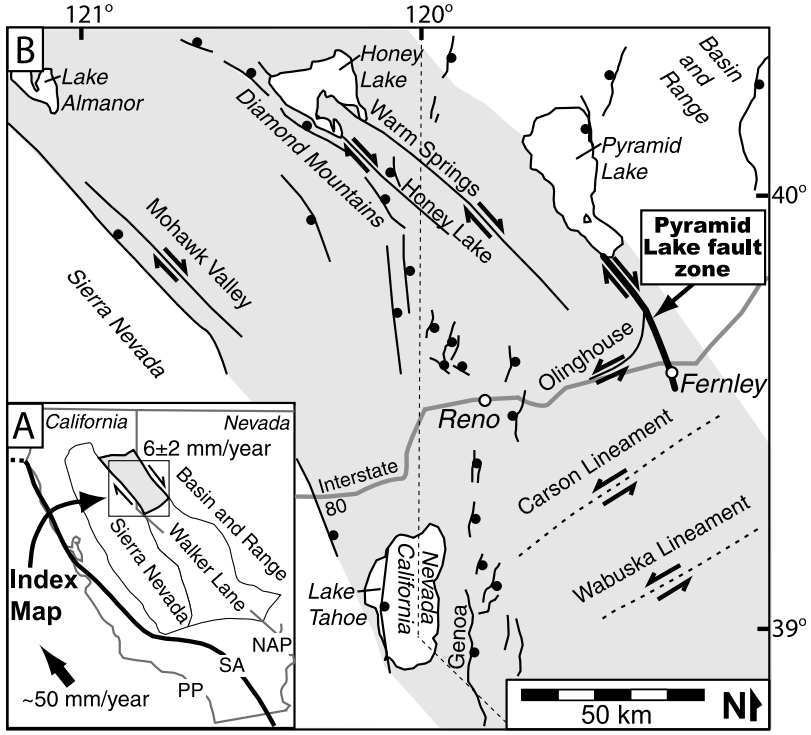

Figure 1. (a) Location of the northern Walker Lane (shaded) with respect to the San Andreas fault (SA) and the Sierra Nevada. Relative plate motion is from *DeMets and Dixon* [1999]. PP, Pacific plate; NA, North America plate. (b) Location of the Pyramid Lake fault zone with respect to known and suspected active faults of the northern Walker Lane. Circle is on the hanging wall of normal faults, and arrows show relative motion across strike-slip faults. Light shaded area denotes the approximate area of the northern Walker Lane.

bounds on the latest Pleistocene and Holocene fault slip rate, earthquake recency, and earthquake recurrence. These observations provide the basis for discussion of the role of the Pyramid Lake fault zone in accommodating right-lateral shear within the northern Walker Lane.

2. Fault Location, Geometry, and General Neotectonic Features

[4] The Pyramid Lake fault zone extends for ~45 km from south of Fernley, Nevada to near the southern tip of Pyramid Lake, where it continues at most another 40 km beneath Pyramid Lake (Figure 2). The active fault trace is nearly linear between Pyramid Lake and Dead Ox wash and is manifested by springs, vegetation and tonal lineaments, tufa deposits, uphill-facing scarps, linear bedrock and alluvial ridges, and an unnamed elongate linear valley containing numerous closed depressions (Figure 3). South of Dead Ox wash, the fault branches into a ~1.5 km wide zone of nested grabens (Figures 3 and 4). The complex surface trace of the fault near Dead Ox wash reflects local extension corresponding to the intersection of the Pyramid Lake fault zone by the conjugate left-lateral Olinghouse fault zone and a change in fault strike from ~N45°W to ~N30°W (Figures 2, 3, and 4). Southward from about Gardella Canyon, the fault is again characterized by a single linear trace across Dodge Flat (Figure 4), where it is expressed as aligned opposite-facing scarps and tonal lineaments in closed playa-filled depressions. The linearity and similarity in strike of the Truckee River just north of Gardella Canyon to the fault strike across Dodge Flat indicates the Truckee River course here is probably fault controlled (Figures 2 and 4).

[5] The fault continues southward through Wadsworth and is marked by a linear arrangement of tonal and vegetation lineaments, scarps, and linear depressions (Figure 4). The southern margin of Dodge Flat forms a terrace riser to the Truckee River and is offset right laterally by the fault. Cultivation and development have obscured potential fault-related geomorphic features in the vicinity of Fernley (Figure 5). The southernmost limit of active faulting we observe is a ~2 km wide, discontinuous series of roughly right-stepping grabens, uphill-facing scarps, and aligned mounds that extend to about seven km south of Fernley (Figure 5).

3. Fault Slip Rates and Earthquake Recency

[6] The trace of the Pyramid Lake fault zone sits almost entirely below the highstand of Lake Lahontan which reached its pluvial maximum at 13,070 ± 60 ^{14}C B.P. (15,475 ± 720 cal. yr B.P.) before rapidly desiccating (Figures 3–5) [*Adams and Wesnousky*, 1999; *Morrison*, 1991; *Benson and Thompson*, 1987] (radiocarbon ages (B.P.) are calibrated to calendar years before present (cal. yr B.P.) using the work of *Stuiver and Reimer* [1993] and *Stuiver et al.* [1998]; all cal. yr B.P. uncertainties represent entire 2-sigma range). The relationship of the northernmost

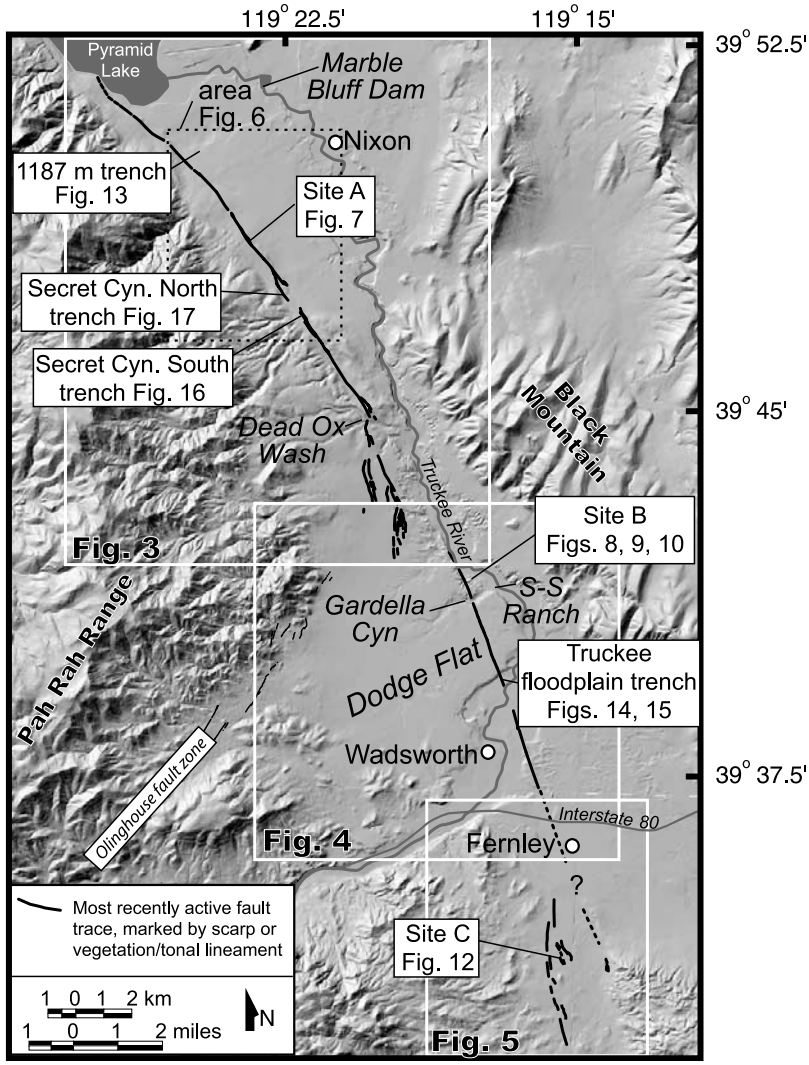

Figure 2. Location of the Pyramid Lake fault zone with respect to Pyramid Lake, Fernley, and Interstate 80. Slip rate sites A–C, trench locations, and outlines of Figures 3–6 are also shown.

portion of the fault to the distribution of late Pleistocene and Holocene deposits is shown in Figure 6. We discuss three sites along the fault where ephemeral stream channels and gullies that formed subsequent to dessication of Lake Lahontan are offset right laterally. The sites are labeled A, B, and C in Figure 2 and are discussed separately below.

3.1. Site A

[7] A topographic map of site A, an offset channel bank, is placed adjacent to the corresponding air photo in Figure 7 (location shown in Figures 2 and 3). At site A, a broad abandoned channel is displaced by two fault strands that form a graben (Figure 7). Right-lateral offset of the abandoned channel is observed along only the eastern fault strand (Figure 7). The northern channel bank is well defined and can be followed into the eastern fault strand, where it is offset right laterally 12–15 m. The southern channel bank is offset a similar amount in the far field but becomes poorly defined close to the fault. The development of the channel, and hence accrual of 12–15 m of offset, postdates desiccation of Lake Lahontan at approximately 15.5 ka. Assuming that multiple earthquakes offset the channel bank, the offset places a minimum limit on the fault slip rate of ~0.7–1.0 mm/year.

3.2. Site B

[8] Canyons formed by headward erosion into the walls of the Truckee River canyon 0.5 km north of Gardella Canyon (site B, Figures 2 and 4) are truncated and offset in a right-lateral sense by the fault (Figure 8). A series of prominent channels and ridges are restored (Figure 9) when right-lateral slip is removed, with the exception of recent headward erosion along channel 1 (Figure 9). Topographic mapping, vertical air photo reconstruction, and field measurements of channel thalweg, channel margin, and ridge crest offsets yield total right-lateral displacement of 35–43 m (Figure 9; site B, Figure 4).

[9] A trench excavated across the fault adjacent to the offset ridges and channels of the side canyons (Figure 10; see Figure 8 for location) confirms the coincidence of the fault strike with the offset side canyons and shows that the fault is characterized here primarily by strike-slip motion, in agreement with nearby surface observations of opposite-facing scarps, linear closed depressions, and lack of significant

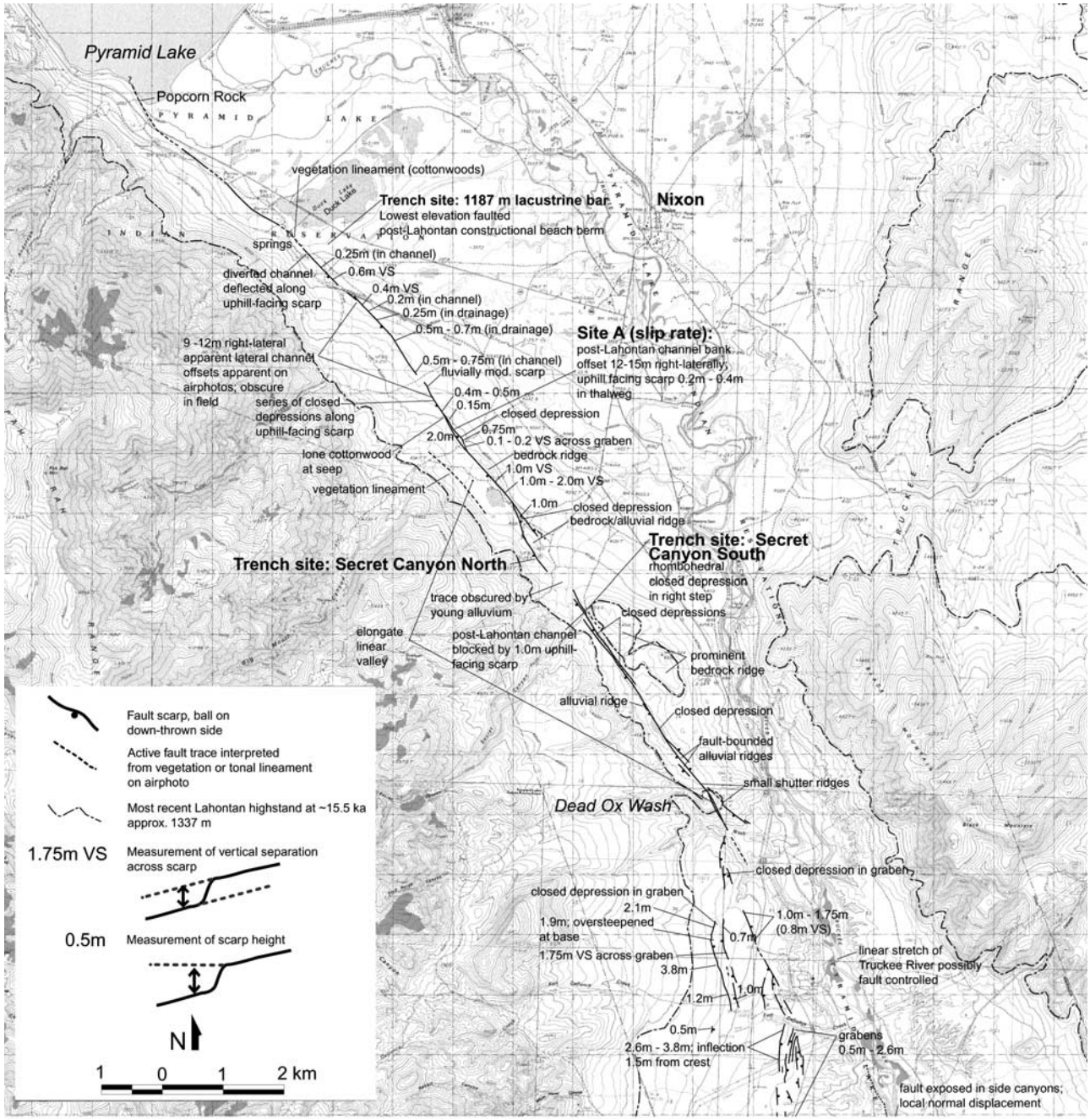

Figure 3. Strip map of scarps and tonal and vegetation lineaments resulting from recent fault activity along the northern portion of the Pyramid Lake fault zone (see Figure 2 for location). USGS 7.5′ topographic quadrangle base. Location is given on Figure 2.

vertical relief across the fault (Figure 4). The oldest deposits exposed in the trench (Figure 10) are lacustrine clayey silts exhibiting a strong columnar structure (unit 1a), capped by thinly laminated lacustrine silts and fine sands (unit 1b). A poorly developed platy soil and thin layer of dendritic tufa are formed on unit 1. Silts and fine sands deposited as thin, continuous laminae (unit 2a) and massive silt and coarse sand with prominent desiccation cracks (unit 2b) rest on the lacustrine sediment of unit 1. The entire exposure is capped by a thick mantle of extensively bioturbated eolian sands and silts (unit 3). The fault zone comprises two primary strands, labeled FW and FE in Figure 10, and several subsidiary strands, labeled a–e. Fault strands FW and FE bound a graben, creating a local closed depression into which fine sand and silts of unit 2 were deposited as subhorizontal thin laminae and subsequently warped. Evidence for lateral motion includes apparent reverse motion across strands b, c, and FW, and a well-developed flower structure showing apparent reverse offset at strand d; vertical to steeply dipping fault orientations throughout the exposure; and significant facies and thickness changes within similar

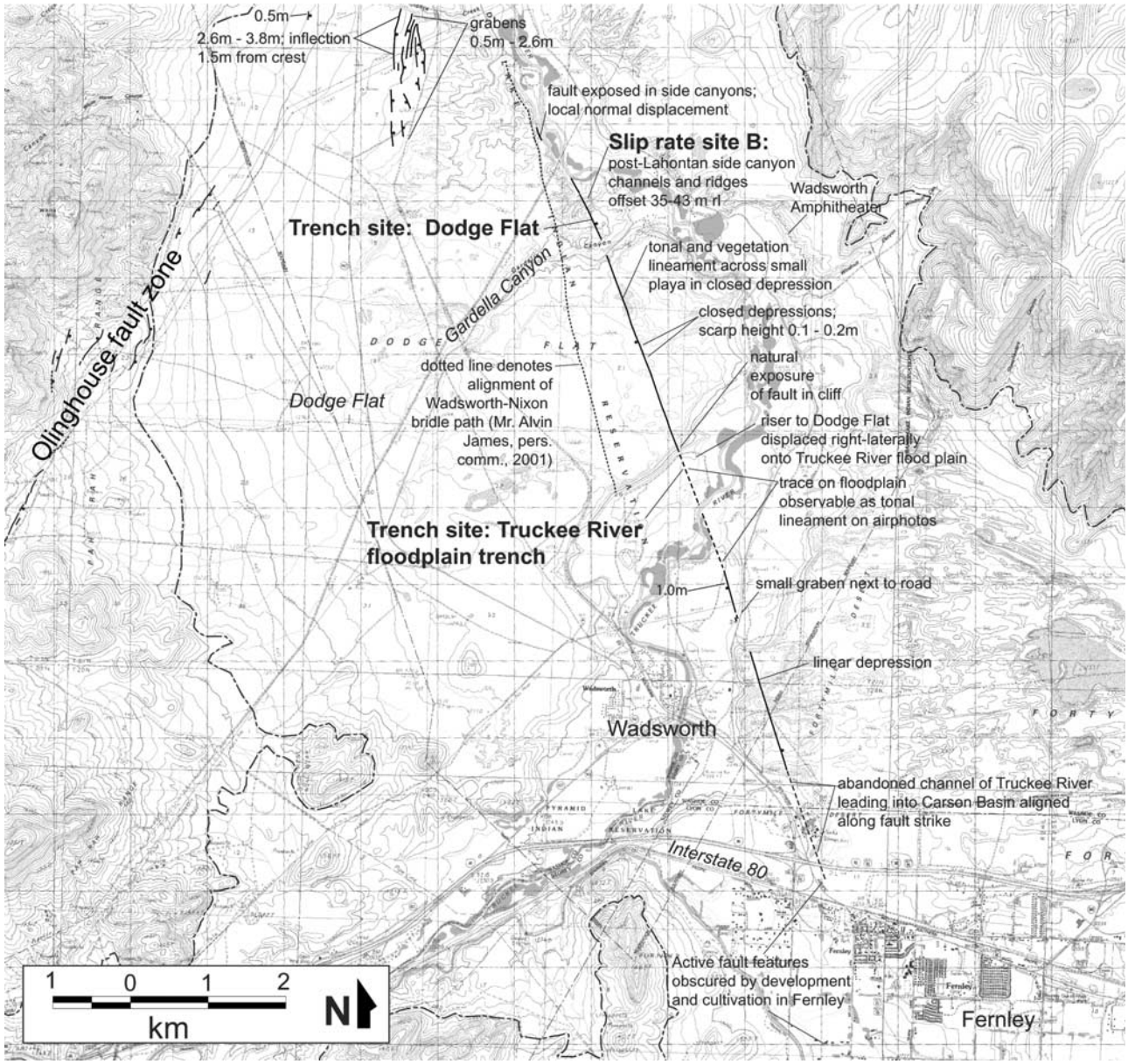

Figure 4. Strip map of scarps and tonal and vegetation lineaments along the central portion of the Pyramid Lake fault zone (see Figure 2 for location). USGS 7.5′ topographic quadrangle base. Legend is as in Figure 3.

units across strands FW, b, c, and d. Total vertical separation across the fault zone is small (0–0.5 m), as determined from displacement of the top of the lacustrine deposits of unit 1b across the graben.

[10] Numerous geomorphic and stratigraphic relations suggest that the Truckee River canyon, and hence the offset side canyons at site B, formed after desiccation of Lake Lahontan at ~15.5 ka. For example, meander scrolls preserved 30 m above modern stream grade near Nixon record the paleoelevation of the Truckee River as Lake Lahontan retreated after ~15.5 ka (Figure 11a). The degree of incision upstream at site B is similar to downcutting at Nixon. Projection upstream of the Nixon meander scroll surface places the Truckee River near the top of the offset side canyons at site B (Figure 11b) during the period when the post-Lahontan meander scrolls at Nixon were formed. Hence the offset features at site B also postdate Lake Lahontan. An apparent absence of inset lacustrine deposits in the Truckee River canyon is also consistent with post-Lahontan canyon incision. The Truckee River may previously have flowed into the Carson Basin [*Jones*, 1933] through a paleochannel along strike of the Pyramid Lake fault zone (Figure 4). Diversion of the Truckee River from the Carson Basin into the Pyramid Basin after ~15.5 ka may have been caused by deflection of the river along contour of post-Lahontan isostatic rebound [*Adams et al.*, 1999].

[11] In summary, the observations reported above point to post-Lahontan formation and offset of the side canyons at site B. Dividing 35–43 m of right-lateral offset measured by

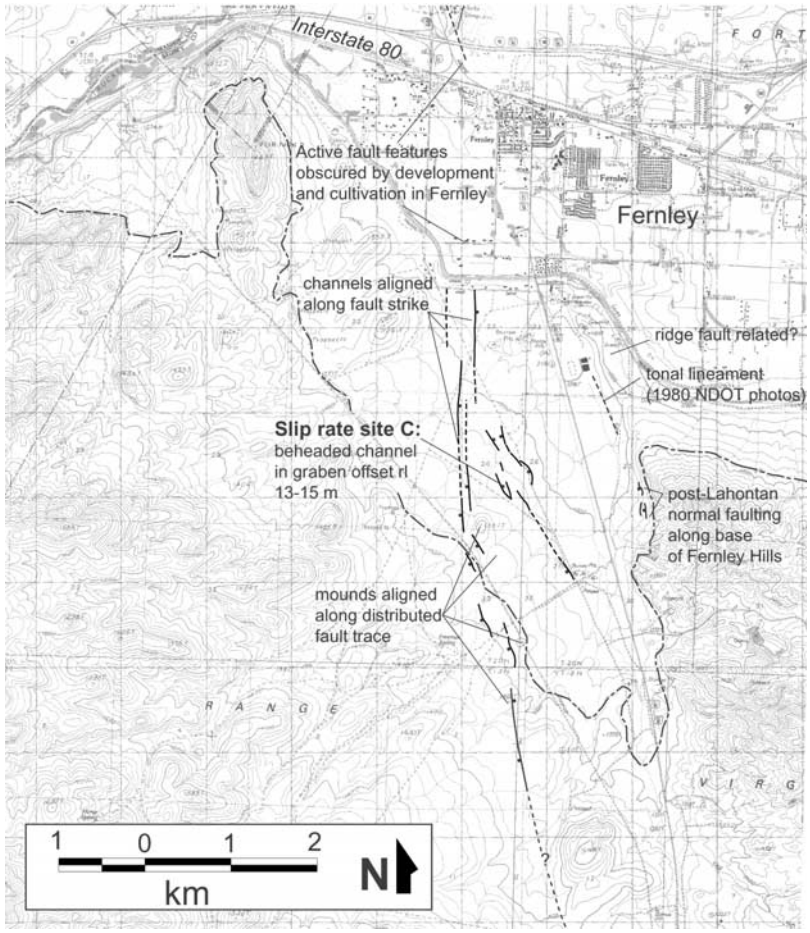

Figure 5. Strip map of scarps and tonal and vegetation lineaments along the southern portion of the Pyramid Lake fault zone (see Figure 2 for location). USGS 7.5′ topographic quadrangle base. Legend is as in Figure 3.

topographic survey and air photo reconstruction by the maximum side canyon age of ~15.5 ka yields a minimum bound on the slip rate of 2.6 ± 0.3 mm/year.

3.3. Site C

[12] A third site, located ~2 km south of Fernley (site C, Figures 2 and 5), preserves a shallow channel formed in post-Lake Lahontan alluvium that is offset 13–15 m in a right-lateral sense and is now beheaded against the fault scarp (Figure 12). Because the fault is distributed and discontinuous here, the offset channel does not record total near-fault deformation. Channel formation and subsequent offset postdates the desiccation of Lake Lahontan (~15.5 ka), and assuming that the feature records multiple earthquakes, the offset provides a minimum slip rate estimate of 0.8–1.0 mm/year.

4. Paleoearthquakes: Recency

4.1. 1187 m Lahontan Constructional Beach Berm Trench

[13] Pyramid Lake reached a historical highstand of ~1185m m during the interval AD 1870–1891 [*Harding*, 1965; *Jones*, 1933]. Surfaces below this elevation are not displaced by the fault and thus postdate the most recent surface rupture (Figure 6). Above this elevation, Lahontan constructional bars are locally buried by post-Lahontan alluvium and faulted. We excavated a small trench (Figure 13) across the lowermost prominent faulted Lahontan constructional beach berm at 1187 m (Figures 2 and 6). The trench exposed lacustrine sands and gravels (unit 2) deposited on alluvial fan debris flow material (unit 1) (Figure 13). A weak soil developed on the buried alluvial fan deposits (unit 1) contained small pieces of detrital charcoal which yielded AMS radiocarbon ages of 4750 ± 120 cal. yr B.P. (sample PLLAC-1187-C1, Table 1) and 4930 ± 100 cal. yr B.P. (sample PLLAC-1187-C2, Table 1). The youngest age obtained, 4750 ± 120 cal. yr B.P., places a maximum bound on the age of the overlying lacustrine gravels of unit 2. Gastropod shells (*Pyrgulopsis nevadensis*) (S. E. Sharpe, Desert Research Institute, personal communication, 2002) collected in situ from the base of the lacustrine deposit (unit 2) yield an AMS radiocarbon age of 3895 ± 165 cal. yr B.P. (Figure 13 and sample PLLAC-1187-G1, Table 1). The age of the shells provides a maximum bound [*Brennan and Quade*, 1997] on the time of last displacement on the Pyramid Lake fault zone, and as well documents a transgression of the lake after ~4 ka.

4.2. Truckee Floodplain Trench

[14] A trench excavated across the fault on a low terrace of the recently active Truckee River floodplain in Wadsworth

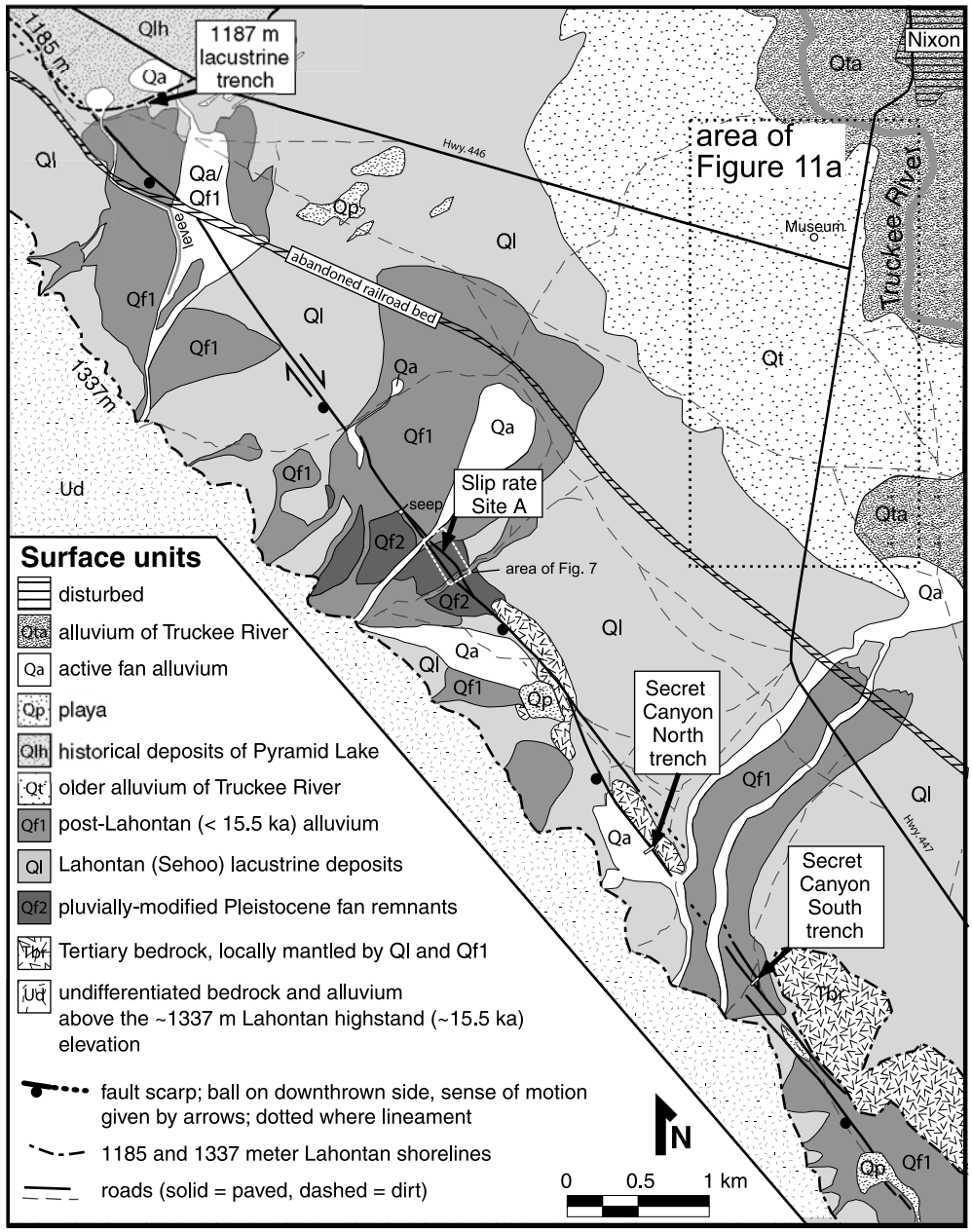

Figure 6. Map showing the relation of the northern portion of the Pyramid Lake fault to surficial deposits (see Figure 2 for location).

(Figures 2 and 4) provides another limit on the recency of faulting. The terrace surface is not displaced by the fault, although the fault trace is visible on older vertical air photos as a tonal and vegetation lineament (Figure 14) due to differential groundwater movement on each side of the buried fault. The oldest deposits exposed in the trench (Figure 15) are fluvial gravels with well-rounded clasts (unit 1). These strata are capped by clay, silt, and fine sand of units 2 and 3 (Figure 15). The fault zone is characterized by one well-developed subvertical strand (strand FE; Figure 15) and a subsidiary strand (strand FW; Figure 15). Fault strands FE and FW juxtapose silty clay (unit 2) against fluvial gravels (unit 1) at the base of the trench. Fault strand FE continues upward and is marked by a clear contrast in texture, color, and weathering characteristics between individual layers of unit 2 across the fault. The entire exposure is capped by an unfaulted flood deposit (unit 3a) along a smooth, planar contact. The uppermost 20–40 cm of the exposure (unit 3b) is a disturbed (ploughed) layer.

[15] Detrital charcoal was obtained in situ from four locations within the faulted fine-grained deposits of unit 2 (Figure 15). AMS radiocarbon dates for the samples are closely grouped between 2245 ± 95 cal. yr B.P. to 1705 ± 175 cal. yr B.P. (samples PLTF-C1 to PLTF-C4; Figure 15, and Table 1). The stratigraphic inversion of these dates within the floodplain deposits is probably the result of reworking of upstream deposits. The youngest charcoal incorporated in unit 2 (1705 ± 175 cal. yr B.P.; sample PLTF-C2, Table 1) represents the maximum age of unit 2. Thus the most recent earthquake preserved in the Truckee

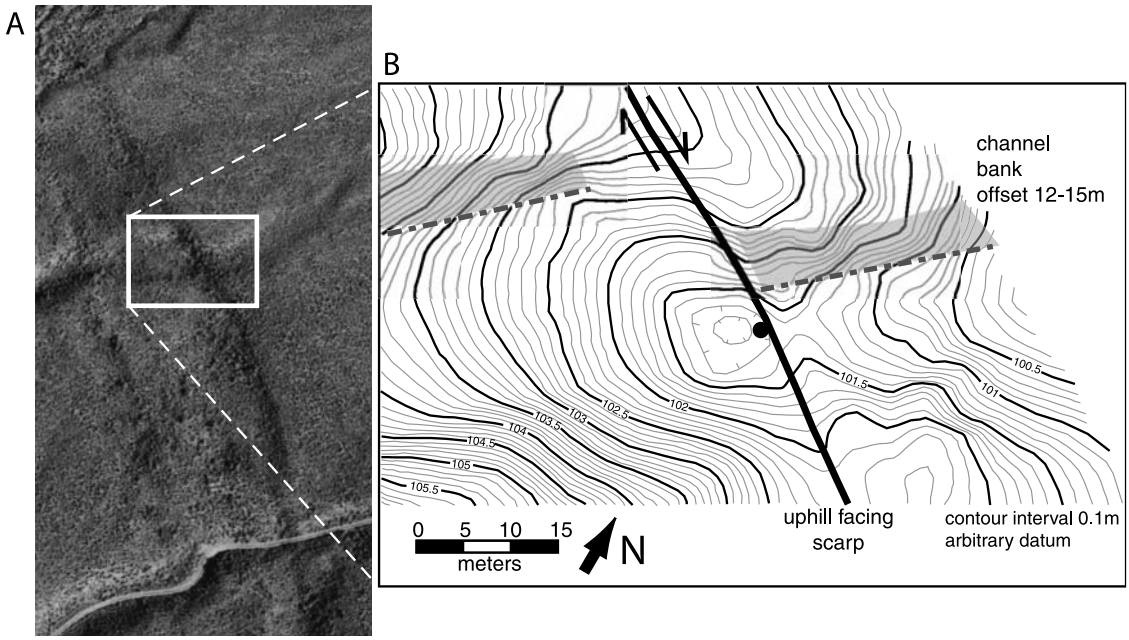

Figure 7. Site A. (a) Vertical low Sun angle air photo and (b) contour map showing offset of channel bank. Total offset is 12–15 m (see Figure 6 for location).

River floodplain trench exposure occurred after 1705 ± 175 cal. yr B.P.

[16] A small (1 × 1 cm) mammal vertebra (J. Auger, University of Nevada, Reno, personal communication, 2002) taken from the unfaulted capping layer (unit 3a) yielded an AMS radiocarbon age of 810 ± 100 cal. yr B.P. (sample PLTF-B1; Figure 15 and Table 1). The sediment of capping unit 3a is of uniform color and texture, lacks internal structure, fines upward, and is interpreted to have been deposited in a single flood event. Assuming the age of the bone closely reflects the age of unit 3a, the most recent surface rupturing earthquake on the Pyramid Lake fault would be before about 810 ± 100 cal. yr B.P. (deposition of unfaulted unit 3) and after 1705 ± 175 cal. yr B.P. (maximum age of faulted unit 2), although it may not be ruled out that the reworked bone is significantly older than the time of deposition of the unfaulted capping layer.

5. Paleoearthquakes: Recurrence

5.1. Secret Canyon South Trench

[17] Two trenches were excavated near Secret Canyon (Figures 2 and 3). The southernmost of these (Figure 16) was placed across a 20–25 m wide, 1.5–2 m deep, rhombohedral graben formed at a local right step of the Pyramid Lake fault zone (Figures 2 and 3). The fault zone is

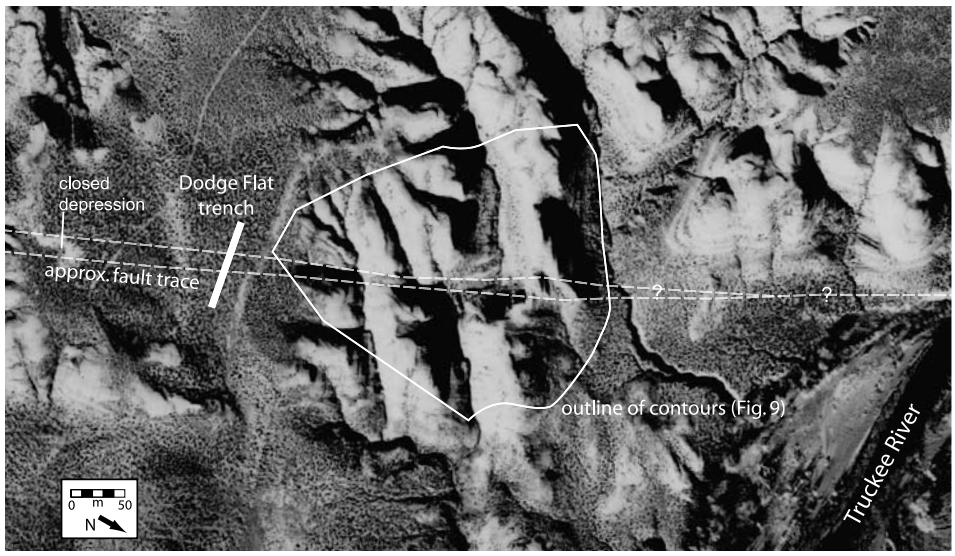

Figure 8. Site B. Vertical low Sun angle air photo showing post-Lahontan highstand (<15.5 ka) side canyons offset by the Pyramid Lake fault (dashed line) and location of Dodge Flat trench.

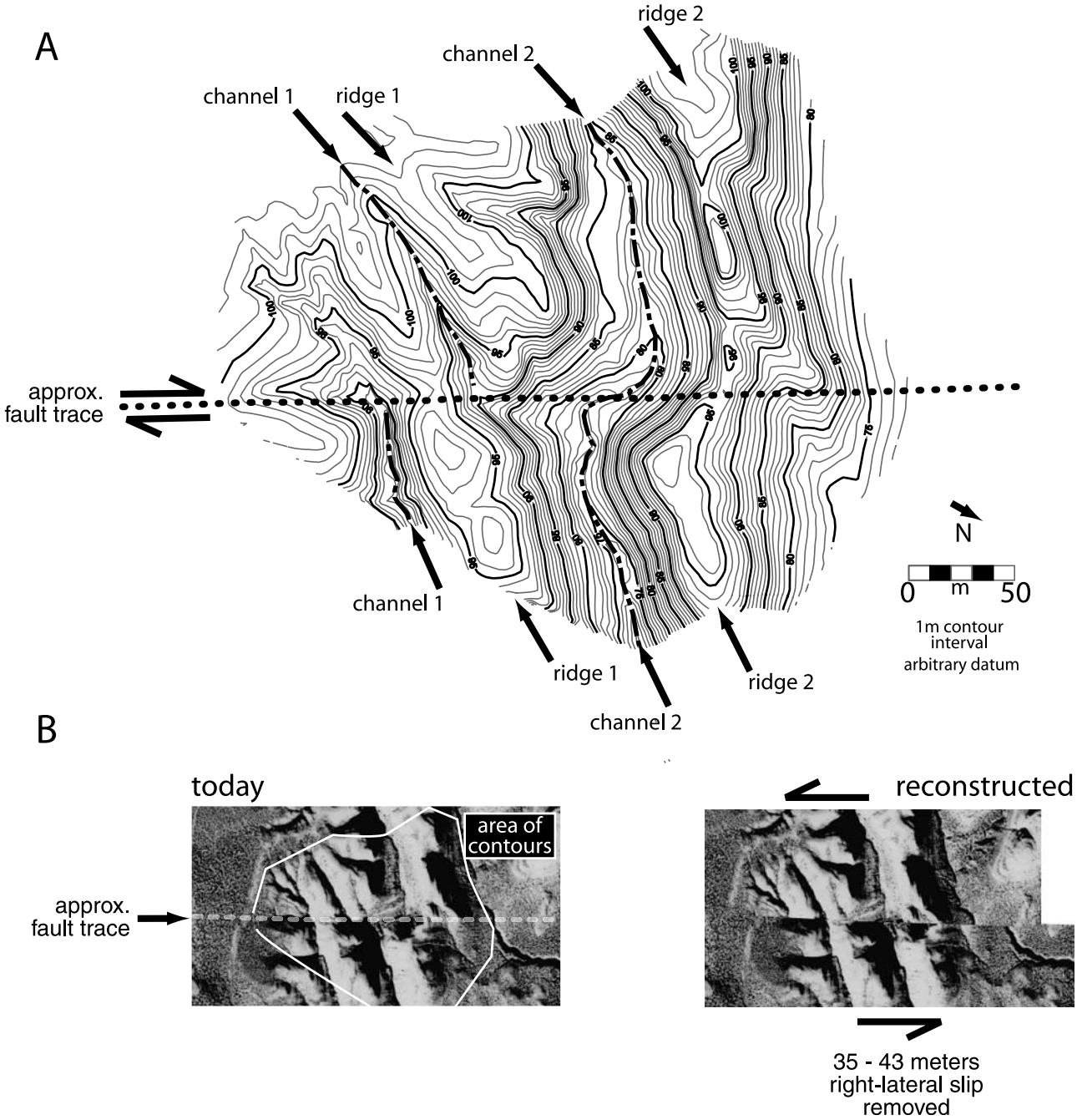

Figure 9. Site B. (a) Topographic map of offset ridges and channels of side canyons at site B. (b) Vertical air photo of offset features showing 35–43 m right-lateral slip restored (see Figures 2 and 4 for location).

characterized by two main strands, labeled FE and FW in Figure 16, and a number of subsidiary strands marked a through h. Strands FE and FW bound the graben. The oldest deposits exposed in the trench (unit 1), east of fault strand FE, are well-sorted lacustrine gravels with well-rounded clasts that exhibit well-developed foresets. These gravels are overlain by poorly sorted debris flow deposits (units 2a and 2b) and a package (unit 3) of interbedded debris flow and alluvial deposits that contain disseminated, reworked Mazama (7627 ± 150 cal. yr B.P.) [*Zdanowicz et al.*, 1999] tephra (A. M. Sarna-Wojcicki, USGS, personal communication, 2002). Subsidiary fault strand a appears to terminate upward within unit 2b, and may record displacement prior to deposition of the Mazama tephra and after deposition of the lacustrine beach gravels of unit 1. The Mazama ash-bearing unit (unit 3) and underlying debris flow deposits (unit 2) are apparently downdropped into the graben along trace FE. Recency of this offset thus postdates ~7.6 ka. Above the tephra-bearing unit 3 and adjacent to the west side of fault FE, there are two packages of colluvium (units C2 and C3) that are interpreted to have been shed off the scarp after two ruptures on fault FE. That

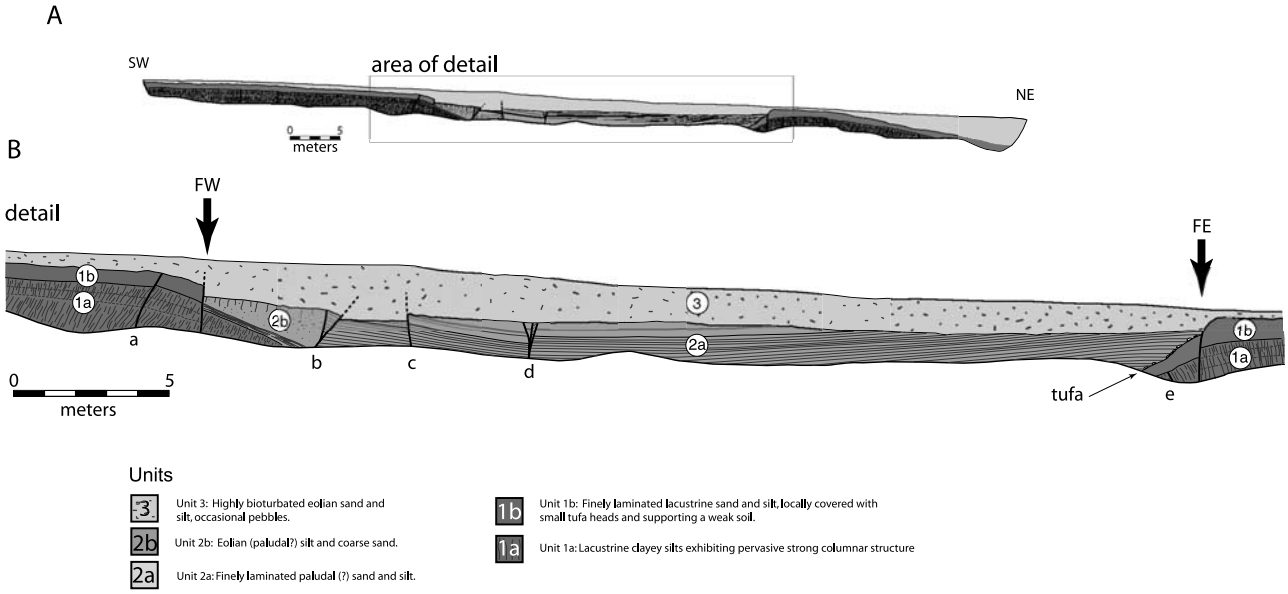

Figure 10. Dodge Flat trench log (see Figures 2, 4, and 9 for location).

colluvial unit C2 represents an earlier event than unit C3 is supported by the observation that colluvial unit C2 has been sheared along the fault plane, whereas unit C3 has not. Subsidiary strand b within the graben is truncated at the horizon that caps colluvial unit C2, and probably reflects the same event. Lower in the section, along fault FE, there is another colluvial unit of material (unit C1) that sits directly below tephra-bearing unit 3. Colluvial unit C1 is interpreted to have been shed off the scarp after a rupture on fault FE, before deposition of the Mazama tephra. Subsidiary strands c, g and h are truncated by the tephra-bearing unit 3 and are interpreted to record the same event that produced colluvial unit C1.

[18] At the western end of the trench, the tephra-bearing unit 3 is displaced downward into the graben along the western fault strand FW (Figure 16). Units displaced across fault FW (units 2, 3, and 4) show significant thickness and facies changes resulting from strike-slip motion. Colluvial packages C2w and C3w are located above the tephra-bearing unit 3. These packages appear to represent the same events as C2 and C3, respectively, based on their shared stratigraphic positions. Subsidiary strands d and e are truncated by colluvial unit C3w, and probably record displacement during the same event that produced unit C3w.

[19] In summary, we observe evidence of three, and possibly four, earthquakes from structural and stratigraphic relations exposed in the Secret Canyon South trench. All earthquakes recorded in the exposure occurred after desiccation of Lake Lahontan at ~15.5 ka. Three earthquakes are represented by the colluvial deposits C1, C2 (and C2W), and C3 (and C3W). Of these, one occurred just prior to deposition of the Mazama ash at approx. ~7.6 ka, while the

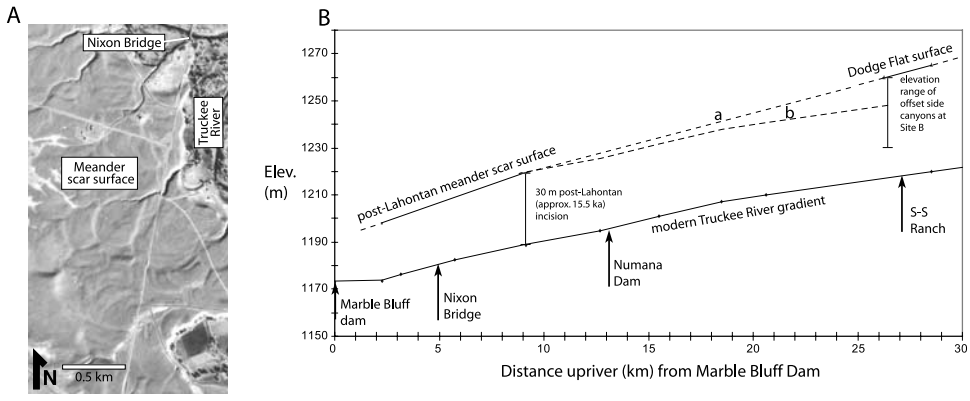

Figure 11. (a) Preserved meander scar surface near Nixon (location on Figure 6). (b) Modern profile of the Truckee River between Marble Bluff Dam and the S-S Ranch (locations on Figure 2), showing up to 30 m of post-Lahontan highstand (~15.5 ka) incision near Nixon and a similar amount of incision at site B. Immediately after desiccation of Lake Lahontan, the Truckee River occupied an elevation between profiles a (connecting meander surface near Nixon with Dodge Flat) and b (modern Truckee River gradient projected from meander scar surface near Nixon) at site B. Elevation data are from USGS 7.5′ topographic quadrangles.

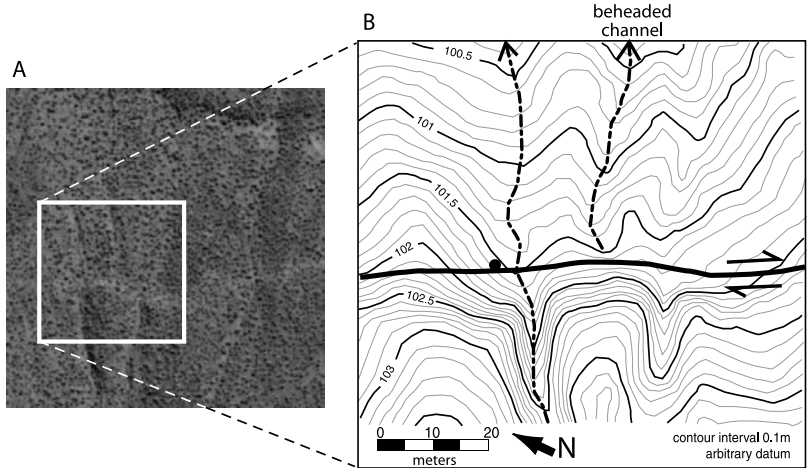

Figure 12. Site C. (a) Vertical low Sun angle air photo and (b) contour map showing beheaded channel. Total offset is 13–15 m (see Figures 2 and 5 for location).

remaining two occurred between ~7.6 ka and the present. An older event that occurred sometime between the last highstand of Lake Lahontan and deposition of the Mazama ash may be preserved along subsidiary strand a, which is ambiguously truncated by unit 2b. Because we are interpreting the earthquake history from vertical offsets but the fault is strike-slip and the stratigraphy coarse, the observations only provide a minimum estimate of the number of events.

5.2. Secret Canyon North Trench

[20] The Secret Canyon North trench (Figure 17) was excavated across the oversteepened base of an ~800 m long, ~10 m high linear alluvial and bedrock ridge (Figures 2 and 3). The fault zone is characterized by two main strands, FE and FW, and subsidiary strands a and b (Figure 17). The western strand (FW) is an east dipping, nearly planar fault exhibiting apparent thrust displacement. The main eastern strand FE opens upward into several splays and shows a significant extensional component. This strand incorporates an ~0.5 m wide zone of fissure fill. The oldest exposed deposits occur east of strand FE and consist of poorly sorted, coarse-grained alluvium with a clay-rich matrix (unit 1a) capped by poorly sorted sands to small cobble gravel with a clay-rich matrix (units 1b–1c), all showing a pervasive shear fabric. The oldest, undated earthquakes in the trench displace unit 1 along subsidiary fault strands a and b. The highly deformed deposits of unit 1 are capped by a poorly sorted clayey silt to small cobble layer with abundant carbonate chips (unit 2a), and poorly consolidated debris flow deposits (unit 2b). Units 1c, 2a, and 2b are apparently downdropped across fault strand FE, where they are capped by eolian silt and sand (units 6 and 7). Sandy silt exhibiting a well-developed vesicular A horizon (Av) caps all exposed deposits (unit 7). The Av horizon is warped downward at the western edge of fault FE, and is buried by a package of coarse slope-derived debris (unit C4). Unit C4 may be colluvium deposited subsequent to downwarping of the Av horizon during the most recent earthquake.

[21] The tilted and highly sheared deposits of the eastern portion of the trench are apparently thrust over more

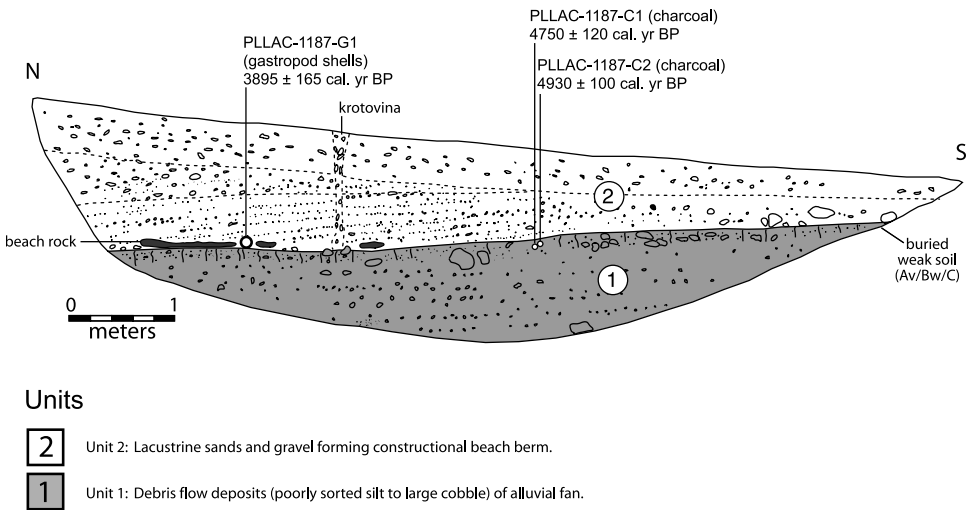

Figure 13. Trench log, 1187 m lacustrine beach berm trench (see Figures 2, 3, and 6 for location).

Table 1. Radiocarbon Data

Sample	CAMS[a] Number	^{14}C Age ± 2σ[b]	δ^{13}C[c]	Calendar Years Before Present (Entire 2σ Range)[d]	Calendar Dates AD/BC (Entire 2σ Range)[d]
PLTF-C1	88198	2135 ± 45	−25	1990–2310	360–40 BC
PLTF-C2	88199	1790 ± 80	−25	1530–1880	AD 70–420
PLTF-C3	90555	2230 ± 40	−25	2150–2340	390–200 BC
PLTF-C4	90554	1915 ± 40	−25	1730–1950	AD 3–220
PLTF-B1	93207	880 ± 35	−19.8	710–910	AD 1040–1240
PLLAC-1187-C1	88191	4235 ± 40	−25	4630–4870	2920–2680 BC
PLLAC-1187-C2	90557	4320 ± 45	−25	4830–5030	3080–2880 BC
PLLAC-1187-G1	93340	3595 ± 35	−1.96	3730–4060	2110–1780 BC
PLFT2-C1	81206	8060 ± 45	−25	8720–9240	7290–6770 BC

[a]Samples processed and AMS ^{14}C measurement performed at Center for Accelerator Mass Spectrometry (CAMS) at Lawrence Livermore National Laboratory.
[b]Using Libby half-life of 5568 years; relative to AD 1950.
[c]Values assumed according to *Stuiver and Polach* [1977] when given without decimal places.
[d]Dendrochronologically calibrated ages calibrated with *Stuiver and Reimer* [1993] (version 4.4) using the work of *Stuiver et al.* [1998].

moderately deformed and undeformed deposits to the west along fault strand FW. Three wedges of colluvium (C1–C3) are interpreted to have shed off or collected against scarps associated with earthquakes on fault FW. Colluvial unit C1 is a wedge-shaped package of poorly sorted sand and angular small cobble and pebbles with chaotic fabric that sits on gently folded lacustrine sands and gravels of unit 3. Farther upsection, a distinctive package (unit C2) of poorly sorted coarse pebbles and rare small cobbles is interfingered with the sand and silt of unit 4c. This package, in turn, is covered conformably by tephra-bearing unit 5, a stratigraphic relationship similar to that observed in the Secret Canyon South trench between a colluvial package (unit C1; Figure 16) and Mazama-tephra-bearing deposits (unit 3 in Figure 16). We interpret the tephra in unit 5 as the Mazama tephra on the basis of its voluminous and continuous character, and its stratigraphic position with respect to underlying Lahontan lacustrine deposits (unit 3) and detrital charcoal (sample PLFT2-C1; 8980 ± 260 cal. yr B.P., Table 1). Above the Mazama-tephra-bearing unit 5, eolian sands and silts of unit 6 are cut by fault FW and a package of coarse-grained sands and pebbles exhibiting a blocky texture and a weak cumulate soil profile (unit C3) sits on the weakly developed soil developed on unit 6. We interpret unit C3 as scarp-derived colluvium resulting from an earthquake that displaced unit 6.

[22] In summary, we observe stratigraphic and structural evidence for three and possibly four post-Lahontan (~15.5 ka) earthquakes in the Secret Canyon North trench. Three earthquakes are represented by colluvial units adjacent to strand FW. The oldest (unit C1) postdates Lake Lahontan but predates deposition of the Mazama tephra (~7.6 ka). Coarse scarp-derived colluvium (unit C2) was deposited after the next youngest earthquake after 8980 ± 260 cal. yr B.P. (sample PLFT2-C1, Table 1) but prior to deposition of the Mazama tephra (~7.6 ka). The next two events postdate deposition of the Mazama tephra. The penultimate event is recorded by fine-grained colluvium (unit C3) derived from unit 6 and bearing a distinctive blocky, cumulate soil. The most recent event may be represented by displacement of unit 7 along a poorly expressed strand of fault FE and capture of coarse slope colluvium (unit C4) between strands FE and FW. Evidence of older, undated pre-Lahontan earthquakes is recorded by possible truncations of small subsidiary strands a and b within highly sheared unit 1. As at the Secret Canyon South site, the number of events recognized is probably a minimum estimate.

6. Discussion and Summary

[23] Post-Lahontan (~15.5 ka) geomorphic features are offset right laterally by the Pyramid Lake fault (Figures 7, 9, and 12). The largest of the observed offsets, 39 ± 4 m (site B; Figure 9) yields a minimum bound on the latest Pleistocene and Holocene slip rate of 2.6 ± 0.3 mm/year. The slip

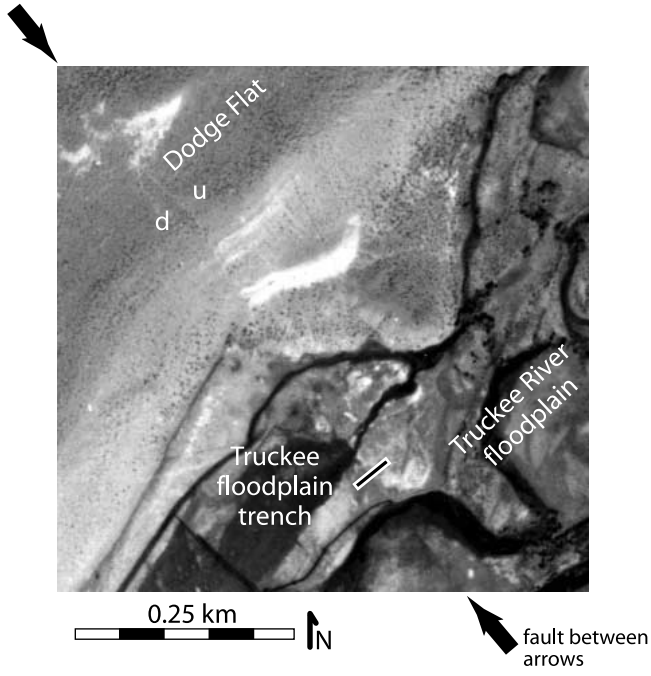

Figure 14. Vertical air photo showing the location of the Truckee River floodplain trench (see Figures 2 and 4 for location) excavated across a tonal lineament on the Truckee River floodplain. Fault steps down from Dodge Flat , where u is relative upthrown and d in relative downthrown sides of fault.

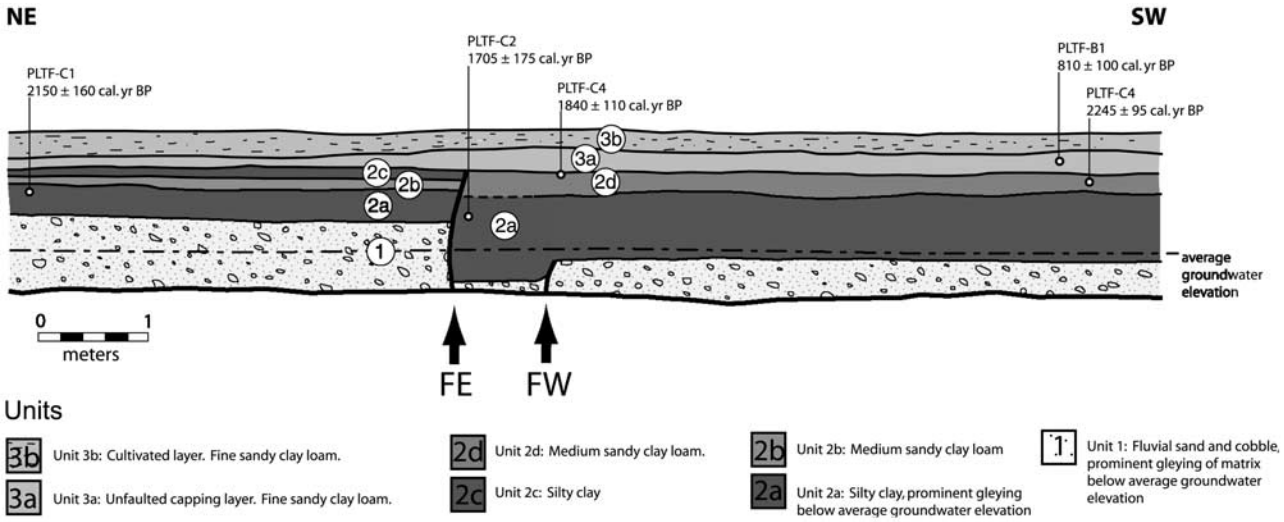

Figure 15. Trench log, Truckee River floodplain trench (see Figures 2, 4, and 14 for location).

rate is a minimum estimate because only the maximum age (~15.5 ka) of the post-Lahontan offset features is known. The rate we obtain is similar to the 1.1–2.7 mm/year minimum slip rate reported previously for the nearby Honey Lake fault zone [*Wills and Borchardt*, 1993], a right-lateral strike-slip fault within the northern Walker Lane of similar orientation and geomorphic expression to the Pyramid Lake fault zone (Figure 1).

[24] The slip rate estimates obtained from sites A, B, and C are all minimum values. The highest minimum value (site B) is located in the central section of the fault whereas those toward the northern and southern ends are lower (sites A and C; Figures 2, 7, 9, and 12). The distribution of rates at sites A–C might be interpreted as an example of an idealized fault slip rate distribution with a central slip rate maximum and rate minima near the tips [*McLeod et al.*, 2000; *Cowie and Roberts*, 2001], but this interpretation is hindered by several factors. Foremost among these is that the rates we obtain are minimum rates because they are estimated from landforms for which only the maximum age is known. Hence the lower rates at sites A and C (Figures 7 and 12) may be apparent because they are derived from features much younger than the feature at site B (Figure 9). Moreover, the endpoints of the Pyramid Lake fault zone are poorly defined, particularly to the north where it strikes underwater. Finally, one slip rate site (site C; Figure 12) is in a wide zone of deformation and almost certainly does not capture the full amount of lateral fault slip.

[25] A maximum bound on the age of the most recent surface rupture of 1705 ± 175 cal. yr B.P. is obtained from the age of faulted deposits exposed in a trench on the Truckee River floodplain (Figure 15). Lacustrine deposits associated with the historical highstand of Pyramid Lake during AD 1870–1890 [*Jones*, 1933; *Harding*, 1965] are not faulted (Figure 6) and provide a limit on the minimum age of the most recent earthquake. If we assume that a bone deposited in an unfaulted capping layer in the Truckee River floodplain trench (Figure 15) closely approximates the date of deposition of the layer, then the most recent earthquake occurred before 810 ± 100 cal. yr B.P. This assumption might not be valid, however, and the most conservative

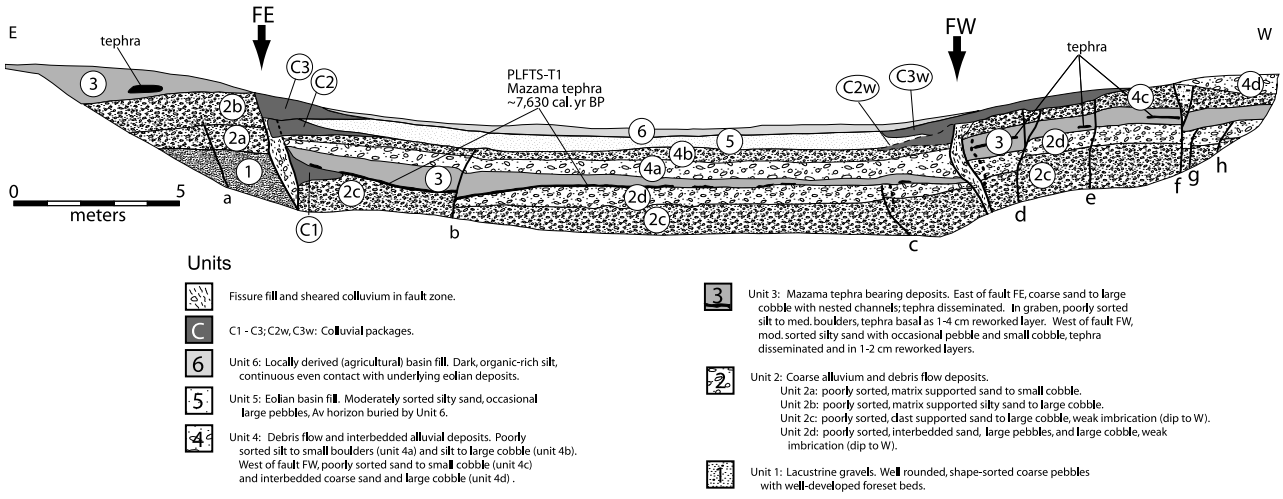

Figure 16. Trench log, Secret Canyon South trench (see Figures 2, 3, and 6 for location).

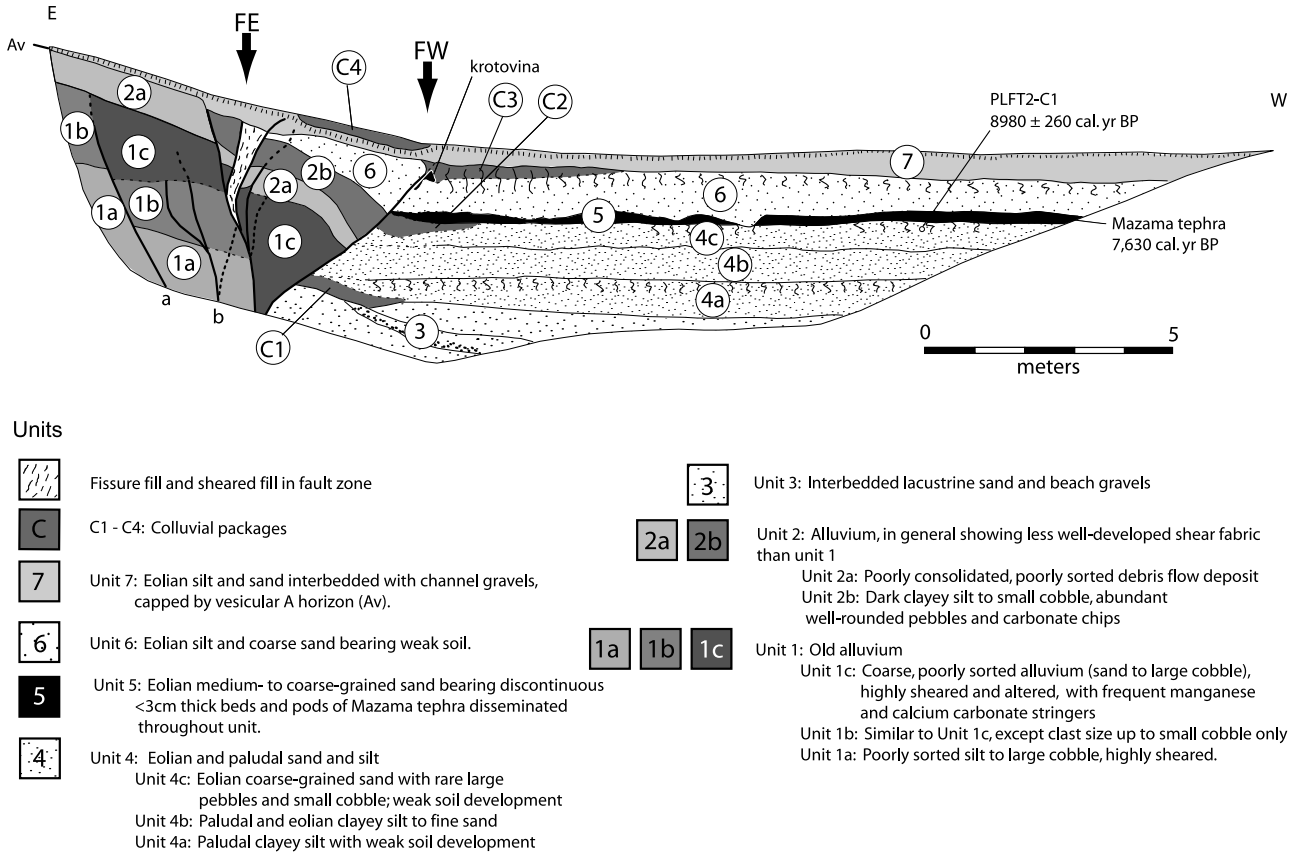

Figure 17. Trench log, Secret Canyon North trench (see Figures 2, 3, and 6 for location).

bracket on the age of the most recent earthquake is between 1705 ± 175 cal. yr B.P. and AD 1880 ± 10.

[26] On the basis of sparse historical records, it has previously been suggested by *Slemmons et al.* [1965] that an earthquake of approximately Ms 7.3 occurred 30 km south of Pyramid Lake in 1845 or 1852, possibly on the Pyramid Lake fault zone. *Ryall* [1977] placed this same event (1845 or 1852) farther to the southeast, not on the Pyramid Lake fault. In 1860, an earthquake of Ml 7.0 [*Slemmons et al.*, 1965] or Ms 6.3 [*Toppozada et al.*, 1981] occurred in western Nevada. Both *Slemmons et al.* [1965] and *Toppozada et al.* [1981] identify the Pyramid Lake fault zone as a possible source for this event. *Anderson and Hawkins* [1984] interpreted a historical earthquake on the Pyramid Lake fault on the basis of qualitative assessments of unfaulted capping deposits in trench exposure. No eyewitness accounts of ground rupture and relatively few felt reports are available to confirm the occurrence of these mid-1800s earthquakes on the Pyramid Lake fault. The fault scarps we observe are relatively subdued, especially in the central (Figure 4) and southern (Figure 5) section of the fault, and there are relatively few unequivocally laterally displaced features over much of the length of the fault. While the possibility that a historical surface rupturing earthquake occurred on the Pyramid Lake fault is allowed by our geologic observations, the 810 ± 100 cal. yr B.P. bone preserved in the unfaulted capping layer of the Truckee trench (Figure 15) suggests to us otherwise.

[27] Stratigraphic and structural relations exposed in three trenches reveal evidence for at least four earthquakes in the past ~15.5 ka (subsequent to the last highstand of Lake Lahontan) (Figure 18). Two trenches, Secret Canyon North and South (Figures 16 and 17), contain evidence for an earthquake that occurred just prior to deposition of the Mazama tephra (~7.6 ka) and two events thereafter. One trench (Secret Canyon North, Figure 17) contains evidence for at least one additional

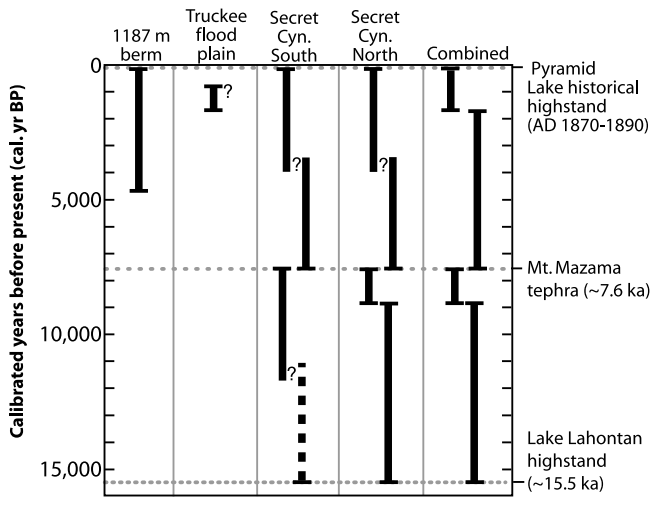

Figure 18. Summary of paleoearthquake timing as interpreted from trench exposures and unfaulted surfaces. Solid bars represent time interval during which each earthquake may have occurred; dashed bar is an ambiguous event.

event prior to deposition of the Mazama tephra (~7.6 ka), but after desiccation of Lake Lahontan, and this event is also suggested by the ambiguous truncation of fault strand a in the Secret Canyon South trench (Figure 16). The timing of the most recent earthquake is limited to between 1705 ± 175 cal. yr B.P. and AD 1880 ± 10 by the maximum ages of faulted floodplain and unfaulted lacustrine deposits (Figures 6 and 15).

[28] A composite of the paleoearthquake records from all trenches (Figure 18) suggests that three earthquakes occurred after 8980 ± 260 cal. yr B.P. with an average recurrence interval of ~2910–3080 years. When combined with our slip rate estimate of 2.6 ± 0.3 mm/year, a recurrence interval of 2910–3080 years implies slip-per-event of 6.7–8.9 m. The range of slip is at the high end or greater than that observed in historical strike-slip earthquakes of similar length (~45–80 km) [e.g., *Wells and Coppersmith*, 1994]. The large values of slip predicted in this manner may reflect incomplete preservation of earthquakes recorded in the coarse stratigraphy of the trench exposures and the use of small vertical components of offset to interpret strike-slip paleoearthquakes in the Secret Canyon trenches (Figures 16 and 17). For example, *Anderson and Hawkins* [1984] interpreted exposures in similar locations on the Pyramid Lake fault zone to indicate a more frequent occurrence of earthquakes, with three or four post-Mazama (~7.6 ka) earthquakes equating to an average recurrence interval of 1900–2530 years. Using the recurrence interval of *Anderson and Hawkins* [1984] and our slip rate estimate of 2.6 ± 0.3 mm/year, the slip accumulated between events would be 5.9 ± 1.5 m, a value similar to maximum displacements associated with the 1990 Landers and 1999 Hector Mine strike-slip earthquakes [*Sieh et al.*, 1993; *Treiman et al.*, 2002] which produced rupture lengths similar to the length of the Pyramid Lake fault zone. The possibility remains that the Pyramid Lake fault zone ruptures in relatively infrequent, but very large earthquakes. If this is the case, sites A and C (Figures 7 and 12) may represent single-event offsets and as such would not record slip rate.

[29] In summary, our observations point to the occurrence of multiple Holocene surface rupturing earthquakes and a minimum late Pleistocene slip rate of 2.6 ± 0.3 mm/year on the Pyramid Lake fault zone. Geodetic surveys indicate that 6 ± 2 mm/year of right-lateral shear strain is accumulating across the Walker Lane at the latitude of the Pyramid Lake fault zone [*Thatcher*, 2003; *Thatcher et al.*, 1999], and hence the Pyramid Lake fault zone appears to accommodate 25–70% of northern Walker Lane shear. Given that the slip rate estimate is a minimum, the percentage may be higher. Thus we conclude that the Pyramid Lake fault zone is the major structure accommodating plate boundary derived right-lateral shear in the northern Walker Lane at ~39°45′N latitude.

[30] **Acknowledgments.** This project was made possible by the interest and support of the Pyramid Lake Paiute Tribe, and we thank the Tribal Council, and in particular Chairman Alan Mandell and Chairwoman Bonnie Akaka-Smith, for permission to conduct this study on tribal lands. Tribal members Alvin James and Wilfred Tobey and families allowed excavation on their ranches; Ben Aleck and Steve Johnson provided archaeological oversight; and Fred John excavated trenches. We also thank Donna Noel and the environmental department. Andrei M Sarna-Wojcicki, Elmira Wan, and Jim Walker provided the tephra correlation, and Saxon Sharpe and Janene Auger kindly donated time and expertise for gastropod test (S.S.) and bone (J.A.) identification. Michaele Kashgarian, Gordon Seitz, and Paula Zermeno performed ^{14}C AMS dating at Lawrence Livermore National Laboratory. For assistance and discussion in the field, we thank Andrew Rael, Senthil Babu Kumar, Mark Engle, Bruce Engle, Jackie Hueftle, Andrew Barron, Thomas Sawyer, Craig dePolo, Alan Ramelli, and Ken Adams. Ken Adams loaned us the air photo in Figure 14, and Andrew 'GIS Jedi' Barron made the shaded relief background for Figure 2. Reviews by James Dolan, Wayne Thatcher, and the Associate Editor Isabelle Manighetti significantly improved this paper. This study was supported in part by USGS NEHRP grant 01-HQ-GR-0186, NSF grant EAR-0001006, and a Geological Society of America Graduate Student Research Grant. Center for Neotectonic Studies contribution 41.

References

Adams, K. D., and S. G. Wesnousky (1999), The Lake Lahontan highstand: Age, surficial characteristics, soil development, and regional shoreline correlation, *Geomorphology*, *30*(4), 357–392.

Adams, K. D., S. G. Wesnousky, and B. G. Bills (1999), Isostatic rebound, active faulting, and potential geomorphic effects in the Lake Lahontan basin, Nevada and California, *Geol. Soc. Am. Bull.*, *111*(12), 1739–1756.

Anderson, L., and F. F. Hawkins (1984), Recurrent Holocene strike-slip faulting, Pyramid Lake fault zone, western Nevada, *Geology*, *12*(11), 681–684.

Atwater, T. (1970), Implications of plate tectonics for the Cenozoic tectonic evolution of western North America, *Geol. Soc. Am. Bull.*, *81*(12), 3513–3535.

Bell, J. W. (1984), Quaternary fault map of Nevada, Reno sheet, *Map 79*, Nev. Bur. of Mines and Geol., Reno.

Bell, E. J., and D. B. Slemmons (1979), Recent crustal movements of the central Sierra Nevada–Walker Lane Region of California-Nevada: Part II, the Pyramid Lake Right-Slip Fault Zone Segment of the Walker Lane, *Tectonophysics*, *52*, 571–583.

Bennett, R. A., B. P. Wernicke, N. A. Niemi, A. M. Friedrich, and J. L. Davis (2003), Contemporary strain rates in the northern Basin and Range province from GPS data, *Tectonics*, *22*(2), 1008, doi:10.1029/2001TC001355.

Benson, L. V., and R. S. Thompson (1987), The physical record of lakes in the Great Basin, in *Geology of North America*, vol. K-3, *North America and Adjacent Oceans During the Last Deglaciation*, edited by W. F. Ruddiman and H. E. Wright Jr., pp. 241–260, Geol. Soc. of Am., Boulder, Colo.

Bonham, H., and D. B. Slemmons (1968), Faulting associated with the northern part of the Walker Lane, Nevada, special paper, 290 pp., Geol. Soc. Am., Boulder, Colo.

Brennan, R., and J. Quade (1997), Reliable Late-Pleistocene stratigraphic ages and shorter groundwater travel times from ^{14}C in fossil snails from the Southern Great Basin, *Quat. Res.*, *47*, 329–336.

Cowie, P. A., and G. P. Roberts (2001), Constraining slip rates and spacings for active normal faults, *J. Struct. Geol.*, *23*, 1901–1915.

DeMets, C., and T. H. Dixon (1999), Kinematic models for Pacific-North America motion from 3 Ma to present: 1. Evidence for steady motion and biases in the NUVEL-1A model, *Geophys. Res. Lett.*, *26*, 1921–1924.

Dixon, T. H., M. Miller, F. Farina, H. Wang, and D. Johnson (2000), Present-day motion of the Sierra Nevada block and some tectonic implications for the Basin and Range province, North American Cordillera, *Tectonics*, *19*, 1–24.

Gan, W., J. L. Svarc, J. C. Savage, and W. H. Prescott (2000), Strain accumulation across the Eastern California Shear Zone at latitude 36°30′N, *J. Geophys. Res.*, *105*, 16,229–16,236.

Harding, S. T. (1965), Recent variations in the water supply of the Great Basin, *Water Resour. Arch. Rep. 16*, Univ. of Calif., Berkeley.

Jones, J. C. (1933), Itinerary, Reno the Pyramid Lake and return, in *Middle California and Western Nevada (Excursion C-1): International Geological Congress, XVI Session, Guidebook 16*, edited by O. P. Jenkins, pp. 102–108, U.S. Gov. Print. Off., Washington, D. C.

McLeod, A., N. H. Dawers, and J. R. Underhill (2000), The propagation and linkage of normal faults: Insights from the Strathspey-Brent-Stratfjord fault array, northern North Sea, *Basin Res.*, *12*, 263–284.

Miller, M. M., D. J. Johnson, T. H. Dixon, and R. K. Dokka (2001), Refined kinematics of the Eastern California Shear Zone from GPS observations, 1993–1998, *J. Geophys. Res.*, *106*, 2245–2263.

Minster, J. B., and T. H. Jordan (1987), Vector constraints on western U.S. deformation from space geodesy, neotectonics, and plate motions, *J. Geophys. Res.*, *92*, 4798–4804.

Morrison, R. B. (1991), Quaternary stratigraphic, hydrologic, and climatic history of the Great Basin, with emphasis on Lakes Lahontan, Bonneville, and Tecopa, in *The Geology of North America*, vol. K-2, *Quaternary*

Nonglacial Geology: Conterminous U.S., edited by R. B. Morrison, pp. 283–320, Geol. Soc. of Am., Boulder, Colo.
Ryall, A. S. (1977), Earthquake hazard in the Nevada region, *Seismol. Soc. Am. Bull.*, *67*, 517–532.
Sieh, K., et al. (1993), Near-field investigations of the Landers earthquake sequence, April to July 1992, *Science*, *260*, 171–176.
Slemmons, D. B., A. E. Jones, and J. I. Gimlett (1965), Catalog of Nevada earthquakes, 1852–1960, *Seismol. Soc. Am. Bull.*, *55*, 519–565.
Stewart, J. H. (1988), Tectonics of the Walker Lane belt, western Great Basin: Mesozoic and Cenozoic deformation in a zone of shear, in *Metamorphism and Crustal Evolution of the Western United States*, *Rubey Vol.*, vol. 7, edited by W. G. Ernst, pp. 683–713, Prentice-Hall, Old Tappan, N. J.
Stuiver, M., and H. A. Polach (1977), Discussion: Reporting of ^{14}C data, *Radiocarbon*, *19*(3), 355–363.
Stuiver, M., and P. J. Reimer (1993), Extended C-14 database and revised CALIB 3.0 C-14 age calibration program, *Radiocarbon*, *35*(1), 215–230.
Stuiver, M., P. J. Reimer, E. Bard, J. W. Beck, G. S. Burr, K. A. Hughen, B. Kromer, F. G. McCormac, J. van de Plicht, and M. Spurk (1998), INTCAL98 Radiocarbon age calibration 24,000 - 0 cal BP, *Radiocarbon*, *40*, 1041–1083.
Svarc, J. L., J. C. Savage, W. H. Prescott, and A. R. Ramelli (2002), Strain accumulation and rotation in western Nevada, 1993–2000, *J. Geophys. Res.*, *107*(B5), 2090, doi:10.1029/2001JB000579.
Thatcher, W. (2003), GPS constraints on the kinematics of continental deformation, *Int. Geol. Rev.*, *45*, 191–212.
Thatcher, W., G. R. Foulger, B. R. Julian, J. Svarc, E. Quilty, and G. W. Bawden (1999), Present-day deformation across the Basin and Range Province, western United States, *Science*, *283*, 1714–1718.
Toppozada, T. R., C. R. Real, and D. L. Parke (1981), Preparation of isoseismal maps and summaries of reported effects for pre-1900 California earthquakes, *Calif. Div. Mines Geol. Open File Rep., 81-11*, 182 pp.
Treiman, J. A., K. J. Kendrick, W. A. Bryant, T. K. Rockwell, and S. F. McGill (2002), Primary surface rupture associated with the Mw 7.1 16 October 999 Hector Mine earthquake, San Bernardino County, California, *Bull. Seismol. Soc. Am.*, *92*(4), 1171–1191.
Ward, S. (1998), On the consistency of earthquake moment rates, geological fault data, and space geodetic strain: The United States, *Geophys. J. Int.*, *134*(1), 172–186.
Wells, D. L., and K. J. Coppersmith (1994), New empirical relationships among magnitude, rupture length, rupture width, rupture area, and surface displacement, *Bull. Seismol. Soc. Am.*, *84*(4), 974–1002.
Wills, C. J., and G. Borchardt (1993), Holocene slip rate and earthquake recurrence on the Honey Lake fault zone, northeastern California, *Geology*, *21*(9), 853–856.
Yount, J., J. Bell, C. dePolo, and A. Ramelli (1993), Neotectonics of the Walker Lane: Pyramid Lake to Tonopah, Nevada, in *Crustal Evolution of the Great Basin and the Sierra Nevada*, edited by M. M. Lahren, J. H. Trexler Jr., and C. Spinosa. pp. 383–391, Geol. Soc. of Am., Boulder, Colo.
Zdanowicz, C. M., G. A. Zielinski, and M. S. Germani (1999), Mount Mazama eruption: Calendrical age confirmed and atmospheric impact assessed, *Geology*, *27*(7), 621–624.

R. W. Briggs and S. G. Wesnousky, Center for Neotectonic Studies, University of Nevada, Reno, NV 89557, USA. (briggs@seismo.unr.edu)